IIETA International Information and Engineering Technology Association
Advancing the World of Information and Engineering

Journal of New Materials for Electrochemical Systems
Vol.23, No.1, January, 2020, pp. 1-6
http://new-mat.org
http://iieta.org/journals/jnmes

To Study the Effect of $LiMn_2O_4$, Nanofibers of $LiMn_2O_4$, and Graphene/Polyaniline/Carbon Nanotube as Electrode Materials in the Fuel Cell

Kabbir Ali[1*], Hafiz Ali Raza[1], Muhammad Irfan Malik[2], Sami Ibn Shamsah[3], Riffat Amna[4] and Amina Sarfraz[5†]

[1] Department of Mechanical Design Engineering, Chonnam National University, Yeosu 550-749, South Korea
[2] Department of Chemical Engineering, College of Engineering, University of Hafr Al Batin, P.O. Box: 1803, Hafr Al Batin, 31991, Saudi Arabia
[3] Department of Mechanical Engineering, College of Engineering, University of Hafr Al Batin, P.O. Box: 1803, Hafr Al Batin, 31991, Saudi Arabia
[4] Department of Chemical Engineering, Khalifa University, Abu Dhabi, United Arab Emirates
[5] COMSATS Institute of Information Technology, Lahore, Pakistan

Corresponding Author Email: *ali_kabbir@hotmail.com, †aminasarfraz20@gmail.com

ABSTRACT

This study is conducted to explore the best electrodes materials for energy conversion devices. The two cathode materials ($LiMn_2O_4$ and nanofibers of $LiMn_2O_4$) and the anode material (graphene/polyaniline/carbon-nanotube) were synthesized by a wet chemical method which includes sol-gel and chemical polymerization techniques. The prepared materials were characterized by SEM, XRD FTIR, and cyclic voltammetry. The characterization results show that $LiMn_2O_4$ exhibits a porous and hollow structure, which improves the utilization of the active mass area, and allows the dual conduction of Li+ and electrons, which effectively relieves the structural strain and volume change. The cyclic voltammetry results record that $LiMn_2O_4$ and nanofibers of $LiMn_2O_4$ as a cathode material enhanced the cycling performance and possess excellent stability. Further, the conductivity of each sample was measured using the DC four-probe method, and the highest conductivity was observed for the $LiMn_2O_4$ nanofibers 1.43 SCm^{-1} at 650°C.

Keywords: *perovskite $LiMn_2O_4$, graphene/polyaniline/carbon nanotube, Fuel cell, Solid oxide fuel cell (SOFC), oxygen reduction reactions (ORR)*

Received: November-29-2019, Accepted: January-06-2020, https://doi.org/10.14447/jnmes.v23i1.a01

1. INTRODUCTION

Population growth, increased industrial development, and advanced computing and digital wireless communication are alarming and could disrupt the energy balance in our eco-environmental system [1-3]. A need for proper and clean energy resources that can be replenished is vital to overcome the energy-related issues. Electrochemical energy devices are the promising devices that fulfill the fast-growing energy needs [4, 5]. There are a variety of clean energy devices ranging from fuel cells to batteries and supercapacitors [6-8]. The fuel cell (FC) system is considered one of the essential candidates composed of high energy densities that are important to fill the demand and supply gap for mobile applications [9-11]. The solid oxide fuel cells (SOFCs) in energy conversion has earned much attention from researchers [12]. However, there are still meaningful efforts needed before full applications of SOFCs in the industry are realized.

The primary limitation in the SOFC is the ionic conductivity of electrolyte and electrode kinetics [13]. Many cathodes and anode materials have been used to improve the energy and power density at a lower temperature [14-17]. The main obstacle to improve the performance is sluggish kinetics of oxygen reduction reactions (ORR), and this is the subject of significant research. Many oxygen-deficient perovskite-structured manganites, ferrites, and cobaltites, have been studied. However, none have reached the conditions of leading catalytic activity for the ORR, high-enough electronic conductivity, and least reactivity with other cell components in the temperature area of interest [18-20]. $La_{1-x}Sr_xMnO_{3-\delta}$ perovskite also has been used as a cathode material because perovskite structure or composite materials are found to be the most effective cathode materials due to their high catalytic activity, However, as the temperature goes below the 800°C, its catalytic activity decreases, thus reducing the cell performance. A new cathode and anode materials are designed with relatively high energy densities and electrochemical performance to overcome this problem [17, 21, 22]. In order to improve the performance of SOFC at low temperatures, it is necessary to fabricate cathode material that possesses higher diffusion rates for oxygen with better kinetics for surface exchange [23, 24]. It has been studied that layered perovskite materials and alkali metals doping in perovskite possessed a fast rate of oxygen diffusion when used as an electrode material and record an improvement in the fuel cells [25-27].

It has numerous vital features like environmentally friendly and flexible design with three-dimensional intercalation capability [28]. The crystalline structure, shape, and grain size of perovskite materials are previously correlated with its electrochemical features [27, 28].

In this work, perovskite $LiMn_2O_4$, nanofibers of $LiMn_2O_4$, and graphene/polyaniline (PANI)/carbon-nanotube were investigated as electrode material in the fuel cell. These materials were synthesized and characterized by different characterization techniques. The surface and structural properties of the synthesized materials were determined using

a variety of methods, including scanning electron microscopy (SEM), X-ray diffraction (XRD), and Fourier-transform infrared spectroscopy (FTIR). The cyclic voltammetry and DC four-probe method used to evaluate the materials' performance based on electrochemical techniques and the properties of the materials were then compared to the electrochemical performance of the electrodes.

2. EXPERIMENTAL PROCEDURE

2.1 Sample preparation

2.1.1 Synthesis of $LiMn_2O_4$

The synthesis of $LiMn_2O_4$ has been carried out by using the traditional Sol-gel method. 0.4 grams of Lithium carbonate salt (Li_2CO_3) was dissolved in 250ml of deionized water and stirred the solution for 2h. Besides that, 18 grams of Manganese nitrate ($MnNO_3$) was added in the solution, and after 1h of further stirring, the desired amount of citric acid (20% of $MnNO_3$) was introduced into the solution to attain the light pink coloration. Later we placed the solution for the gelation process, which was then dried at 800℃ in a muffle furnace to carry out the sintering process. The sintered product obtained was ground in the powder form using the pestle and mortar.

2.1.2 Synthesis of $LiMn_2O_4$ nanofibers

The $LiMn_2O_4$ nanofibers were synthesized by the Electrospinning method. 0.4 grams of lithium acetate $Li(CH_3COO)_2.4H_2O$ and 2 gram of manganese acetate $Mn(CH_3COO)_2.4H_2O$ were added in 10ml of deionized water and stirred vigorously for 4h to attain the good dispersion. Then the 40ml of 10wt% aqueous polyvinyl alcohol (PVA) solution introduced slowly in the suspension under the continuous stirring to obtain the viscous solution of lithium acetate, manganese acetate, and PVA. Then electrospinning of viscous solution has been carried out by using an aluminum foil as a collector. A 20KV high voltage across the collector was applied to obtain the nanofibers, and metal needle distance was maintained at 20cm. Finally, the precursor collected at collector was dried at 70℃ for 4h and calcined at a different heating rate to get $LiMn_2O_4$ nanofibers.

2.1.3 Synthesis of graphene polyaniline CNT

Graphene polyaniline (PANI)/carbon nanotubes were prepared by chemical polymerization. The desired amount of the CNTs were stirred for 30 minutes in a mixture of 270ml of water and 30ml of HCl. Later two samples of ninety (90) ml solutions were withdrawn from the CNTs suspension, and 0.5g of graphene and 3ml of polyaniline were introduced in samples separately. Later, another batch of 120 ml suspension was prepared with the addition of 0.7g ammonium persulphate $(NH_4)_2S_2O_8$. All three different samples were stirred for 2h separately. After that, two 90ml solutions were mixed and placed on the ice bath under the constant stirring for 4h. Later the 120ml of ammonium persulphate solution was added as a dropwise until its color changes from green to blue. Finally, the suspension was filtered and dried at 60℃ for 3h, and the dried product was ground to obtain the graphene/ polyaniline/CNT.

2.2 Sample characterization

Surface and structural properties with varying compositions of the materials were characterized by different characterization techniques and correlated with the electrodes' electrochemical performance. The crystal structure of the materials was determined using an X-ray diffractometer with Cu-Kα radiation. Fourier Transform Infrared Spectroscopy (FTIR) was used to determine the presence of different functional groups. The samples' surface morphology was investigated on Scanning Electron Microscope (SEM), while Cyclic Voltammetry and impedance curves examined the electrochemical behavior of the materials. A DC 4-probe method was used to observe the conductivity in the prepared samples, and the Arrhenius curve plot computed the activation energy of the surfaces.

3. RESULTS AND DISCUSSIONS

3.1 Phase analysis/crystal structure

Figure 1 shows the XRD pattern for $LiMn_2O_4$. All the central diffraction peaks for $LiMn_2O_4$ are indexed by the cubic structure corresponding to crystal planes of (111), (311), (222), (400), (331), (511), (440), (531), (533) and (622) respectively. The crystallite size for the synthesized material was calculated by using Scherer's formula for the strongest diffraction peak corresponding to (111) at

$$D = \frac{0.94\lambda}{\beta Cos\theta}$$

where, θ is the diffraction angle, λ is X-rays wavelength, and β is FWHM of the peak. The average crystallite size calculated for the cubic structure of $LiMn_2O_4$ was approximately 42nm, which is in good agreement with the literature review.

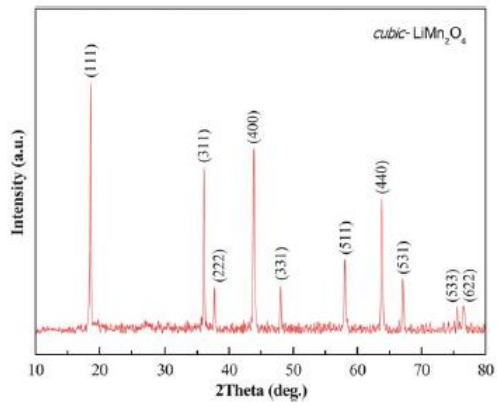

Figure 1. XRD pattern for $LiMn_2O_4$

3.2 FTIR analysis

FTIR analysis was carried out to study the attachment of different functional groups in the synthesized materials. Figure 2(a), (b), and (c) shows the FTIR spectra for $LiMn_2O_4$ prepared by Sol-gel method, $LiMn_2O_4$ Nanofibers, and graphene/polyaniline (PANI)/carbon nanotubes respectively. The FTIR-Spectrum of Lithium manganese oxide ($LiMn_2O_4$) synthesized by the sol-gel method at 6500C in Figure 2(a) was studied at different frequencies, 826.75, 994.88, 1118, and 1631.68 cm^{-1}, respectively the absorption bands in the FTIR spectra confirmed the metal-oxygen (Mn-O) vibrational

frequencies. The high-frequency bands are associated with asymmetric stretching modes of the MnO_6 group. It is also estimated that vibrational frequencies of alkali metal cations in their octahedral sites lie in the frequency range from 200-400cm^{-1} but, further study reveals that vibrational modes of transition metals lie in the frequency range from 400-1000cm^{-1}.

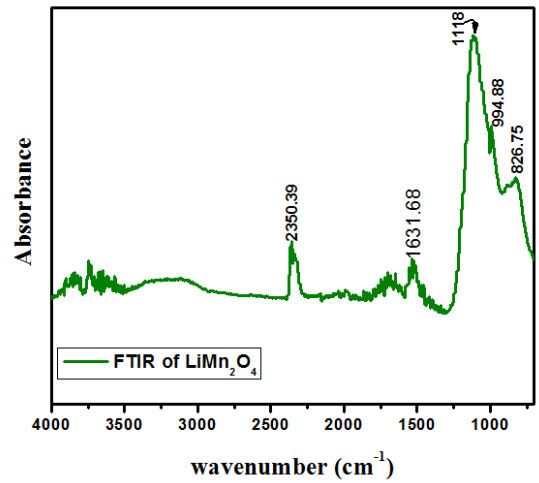

(a)

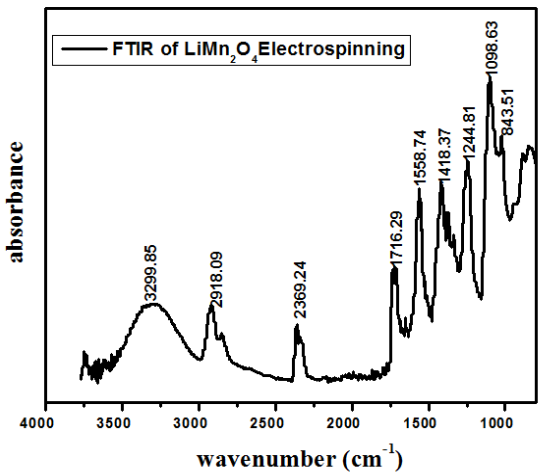

(b)

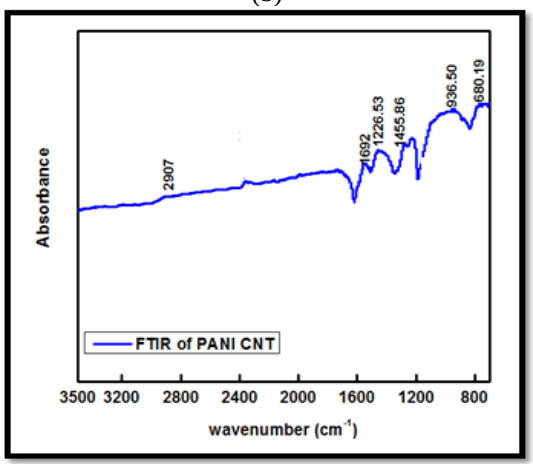

(c)

Figure 2. (a) FTIR spectra for $LiMn_2O_4$ (b) FTIR spectra for $LiMn_2O_4$ nanofibers (c) FTIR spectra for graphene/polyaniline (PANI)/carbon nanotubes

Figure 2 (b) shows the Fourier transform infrared (FTIR) absorbance spectra in the region of 1000-4000 cm^{-1} for the $LiMn_2O_4$ nanofibers calcined at 70 ℃. As shown in the figure, peaks at 3299, 2918, 1716, 1558, 1418, 1244, 1098, and 843 cm^{-1} correspond to $\nu_{s.-H}$, ν_{c-c}, ν_{c-o}, ν_{o-H}, and ν_{Li}-CH3COO respectively. These peaks are generated due to the decomposition of PVA, $Li(CH_3COO).2H_2O$, and $Mn(CH_3COO).4H_2O$. Two major asymmetric stretching peaks are at 1098, and 1244 cm^{-1} corresponds to the MnO bonds present in MnO6. The stretching at 608 cm^{-1} relates to the O-Mn4+-O, and stretching's at 510 represents Mn3+-O; these two stretchings are possible in the $LiMn_2O_4$ spinel structure. However, Li-O vibrational motion, which is challenging to identify, is located in the frequency range of 900-500 cm^{-1}.

The FTIR spectrum from 800 cm^{-1} to 3500 cm^{-1} showed in Figure 2(c). represents graphene/polyaniline (PANI)/carbon nanotubes synthesized by chemical polymerization at 800℃. The peak at 1455 cm^{-1} indicate the stretching vibration of the COOH group, and the peak originated at 1692 cm^{-1} and 1226 cm^{-1} related to the IR active phonon mode of CNTs and the C-N stretching vibration of an aromatic conjugation respectively. The defect side of CNTs found very sensitive to atomic interactions.

3.3 Microstructure/morphology

Figure 3 (a), (b), and (c) indicates the morphological structure of $LiMn_2O_4$, $LiMn_2O_4$ Nanofibers, and graphene/polyaniline (PANI)/carbon nanotubes, respectively. SEM image of 500nm and 20µm $LiMn_2O_4$ particles are shown in Figure (a), and it is observed that all samples are distributed un-uniformly. Large particle surfaces are covered with smaller grains, which confirmed that the nucleation and growth process dominated the particle morphology and revealed that particles have different morphology with an average particle size of 10-20µm. The SEM micrographs also show that surface morphology is quasi-spherical, and there is also a little agglomeration of powder samples, which is due to citric acid. The properties mentioned above are very suitable to use the synthesized material as an electrode in the Fuel cell.

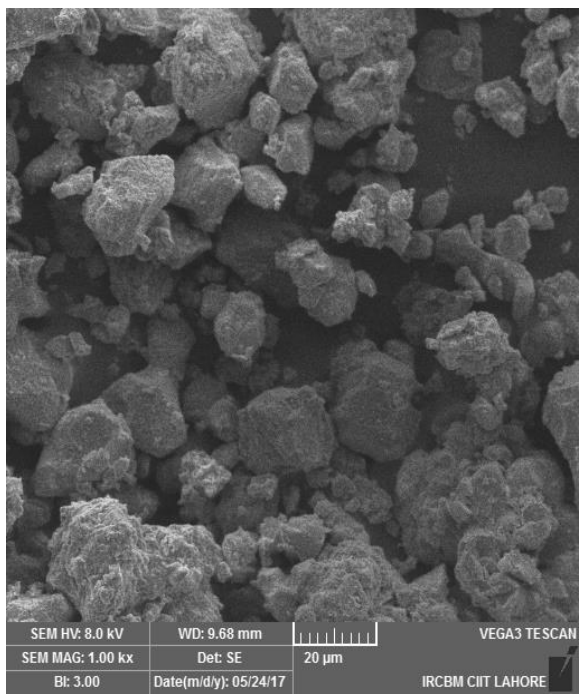

(a)

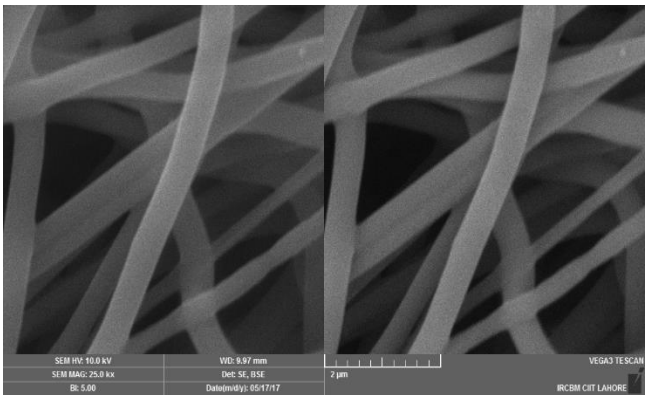

(b)

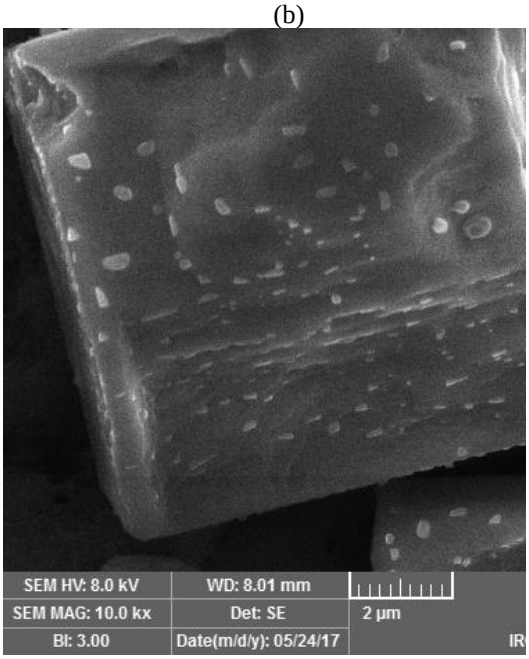

(c)

Figure 3. (a) SEM image for $LiMn_2O_4$ particles (b) SEM image for $LiMn_2O_4$ nanofibers (c) SEM image for graphene/polyaniline (PANI)/carbon nanotubes

The SEM images of $LiMn_2O_4$ fibers calcined at 70℃ are shown in Figure 3 (b). The surface of PVA, lithium acetate, and manganese acetate composite fibers are smooth due to their amorphous nature, as confirmed in Figure 3 (b). The nanofiber diameter range is from 2-100µm, which established a high aspect ratio. There is no visible bead formation in the as-spun fiber, which reveals that the fibrous precursor has been synthesized under optimized conditions. The prepared electrospun membranes have fully interconnected multifiber layers with porous structures because interlayer of multifiber layers generated a nano-/micro porous structure between the ultrafine in electrospun polymer and nanocomposite polymer blend that might be absorbed and retained more electrolytes effectively.

3.4 Conductivity measurements

Figure 4 shows the conductivity measurements of $LiMn_2O_4$, $LiMn_2O_4$ Nanofibers, and graphene/polyaniline (PANI)/carbon nanotubes by DC four-probe method from 250℃ to 650℃. The measurements were plotted between temperature (T) and conductivity (σ), and it is observed that the conductivity of all the synthesized samples increased with the rise in temperature. The highest conductivity values are found for $LiMn_2O_4$ nanofibers, which is 1.43 SCm^{-1} at 650℃. Similarly, $LiMn_2O_4$ and graphene/polyaniline (PANI)/carbon nanotubes showed a conductivity of 1.26 SCm^{-1} and 1.23 SCm^{-1}, respectively, at 650℃.

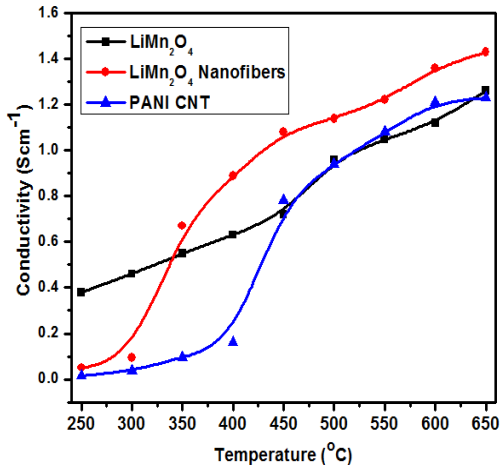

Figure 4. Conductivity measurements for synthesized materials

3.4.1 Electrical bandgap analysis

In Figure 5 (a), (b) and (c) Arrhenius plots are shown to calculate the electrical bandgap for all synthesized materials. The bandgaps are calculated by the Arrhenius equation using conductivity measurements as follows.

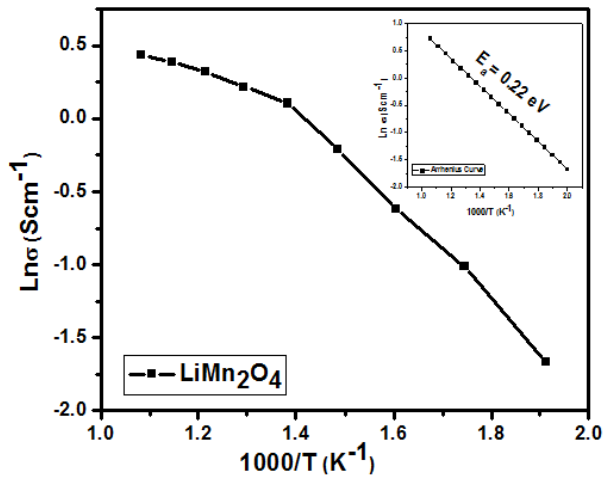

(a)

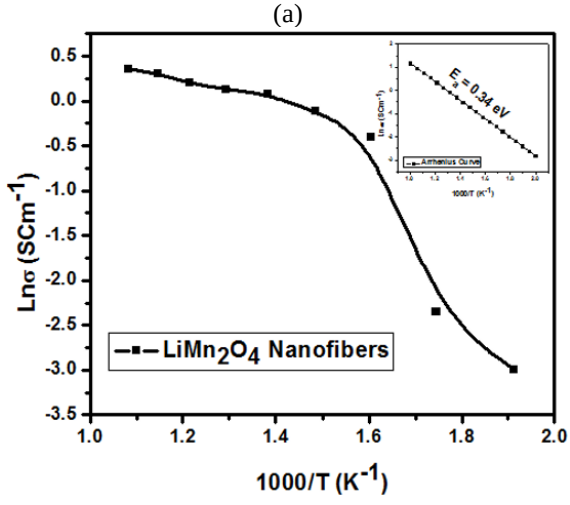

(b)

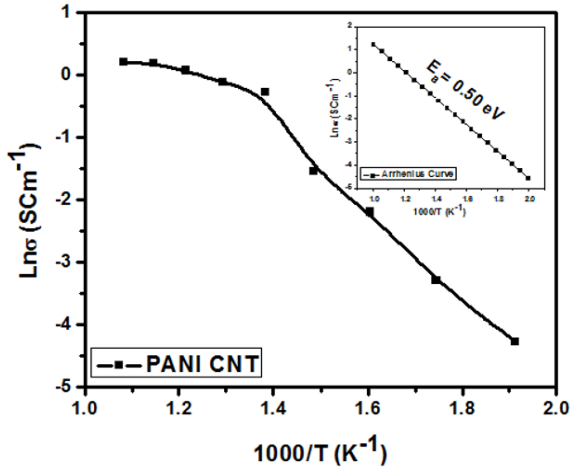

(c)

Figure 5. Arrhenius plot for all synthesized materials

$$\sigma = \sigma_o \exp(-E_a/RT)$$

where,

$$\text{Slope} = -E_a/R$$

Ea is the activation energy, and electrical bandgap is two times of activation energy

$$\text{Electrical bandgap} = 2E_a$$

The bandgaps of $LiMn_2O_4$ particles, $LiMn_2O_4$ nanofibers, and graphene/polyaniline (PANI)/carbon nanotubes were 0.44ev, 0.68ev, and 1ev, respectively. These bandgaps show that all the materials have good potential to be used in energy conversion devices. The electrical bandgap and activation energy for all synthesized materials were calculated in electron volt (eV).

3.5 Cyclic voltammetry

Cyclic voltammetry (CV) was performed to observe the performance of the working electrode ($LiMn_2O_4$ thin film) and the reference electrode (graphene/polyaniline (PANI)/carbon nanotubes).

Figure 6 shows the capacitance behavior of electrode films deposited on the graphite substrate with a potential range of -0.5 to 1.5 V at different scans of 5, 25, 50, and 100 mvs^{-1}. The CV curves exhibited a hysteresis loop shape with no apparent peaks. It has been noticed that current density was continuously increasing with the rise in the scan rate, and the highest current peak was recorded at 100 mv/s.

The electrode's specific capacitances are measured and shown in Table 1 at different scan rates using the following equation.

$$C = I/S\ (m_1+m_2)$$

where, I is the specific current, S is the scan rate, and m_1, m_2 are the masses of two electrodes.

Table 1 concludes that specific capacitance and scan rates are inversely proportional to each other. At the lower scan rate, many electrolyte ions travelled to the electrode's surface, which eventually increased the capacitance. In contrast, at a high scan rate, electrolyte ions do not effectively access the electrode materials and faced a high resistance, which ultimately decreased the capacitance.

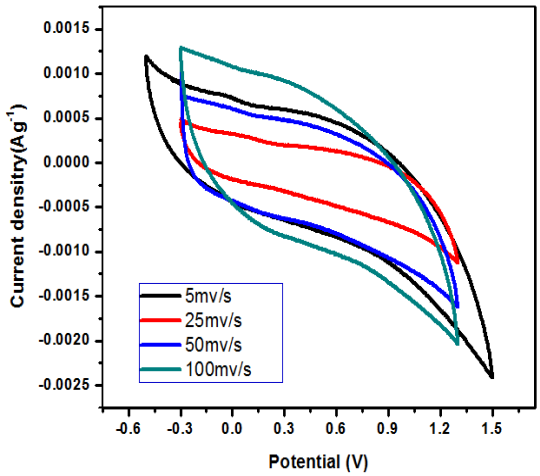

Figure 6. Cyclic voltammetry at different scan rates

Table 1. Specific capacitance of cycle at different scan rates

Scan rate (mv/s)	Specific capacitance F/g
5	0.0536
25	0.0107
50	0.0053
100	0.0026

4. CONCLUSION

In this work, two different cathode materials ($LiMn_2O_4$ and nanofibers of $LiMn_2O_4$) and one anode material (graphene/PANI/carbon nanotubes) were synthesized. The graphene/PANI/carbon nanotubes based anode showed high conductivity, tailored the electron transport within the electrode material, and enhanced the lifetime with high rate capability, which leads to suitable specific capacitance at lower scan values. The graphene nanosheets and carbon nanotubes assembly in graphene/PANI/carbon nanotubes behave as molecular wire to transport the electrons with high standards of electrochemical behavior and good current density as confirmed by the Cyclic voltammetry (CV). Similarly, $LiMn_2O_4$, as a cathode, the material exhibits good cycle life and high capacity. The porous and hollow structure of $LiMn_2O_4$ improves the utilization of active mass, allows dual conduction of Li+ and electrons, and effectively relieves the structural strain and volume change, which ultimately enhanced the cycling performance and rate stability. DC four-probe method showed the highest conductivity of 1.43 SCm^{-1} for $LiMn_2O_4$ nanofibers at 650°C.

REFERENCES

[1] Kothari, D.P., Signal, K.C., Ranjan, R. (2011). Renewable Energy Sources and Emerging Technologies. PHI, 2nd Revised Edition.

[2] Bull, S.R. (2001). Renewable energy today and tomorrow. Proceedings of the IEEE, 89(8): 1216-1226. https://doi.org/10.1109/5.940290

[3] Kaygusuz, K. (2002). Renewable and sustainable energy use in Turkey: A review. Renewable and Sustainable Energy Reviews, 6(4): 339-366. https://doi.org/10.1016/S1364-0321(01)00007-7

[4] Sheikh, M.A. (2010). Energy and renewable energy scenario of Pakistan. Renewable and Sustainable Energy Reviews, 14(1): 354-363. https://doi.org/10.1016/j.rser.2009.07.037

[5] Malik, M.I., Malaibari, Z.O., Atieh, M., Abussaud, B. (2016). Electrochemical reduction of CO_2 to methanol over MWCNTs impregnated with Cu_2O. Chemical Engineering Science, 152: 468-477. http://dx.doi.org/10.1016/j.ces.2016.06.035

[6] Burke, A.F. (2007). Batteries and ultra-capacitors for electric, hybrid, and fuel cell vehicles. Proceedings of the IEEE, 95(4): 806-820. https://doi.org/10.1109/JPROC.2007.892490

[7] Sengodan, S., Lan, R., Humphreys, J., Du, D., Xu, W., Wang, H., Tao, S. (2018). Advances in reforming and partial oxidation of hydrocarbons for hydrogen production and fuel cell applications. Renewable and Sustainable Energy Reviews, 82: 761-780. https://doi.org/10.1016/j.rser.2017.09.071

[8] Jacobson, A.J. (2010). Materials for solid oxide fuel cells. Chemistry of Materials, 22(3): 660-674. https://doi.org/10.1021/cm902640j

[9] Shao, Z., Haile, S.M. (2004). A high-performance cathode for the next generation of solid-oxide fuel cells. Nature, 431: 170-173. https://doi.org/10.1038/nature02863

[10] Park, S., Vohs, J.M., Gorte, R.J. (2000). Direct oxidation of hydrocarbons in a solid-oxide fuel cell. Nature, 404(6775): 265-267. https://doi.org/10.1038/35005040

[11] Brett, D.J., Atkinson, A., Brandon, N.P., Skinner, S.J. (2008). Intermediate temperature solid oxide fuel cells. Chemical Society Reviews, 37(8): 1568-1578. https://doi.org/10.1039/B612060C

[12] Ormerod, R.M. (2002). Solid oxide fuel cells. Chemical Society Reviews, 32(1): 17-28. https://doi.org/10.1039/b105764m

[13] Ralph, J.M., Schoeler, A.C. Krumpelt, M. (2001). Materials for lower temperature solid oxide fuel cells. Journal of Materials Science, 36: 1161-1172. https://doi.org/10.1023/A:1004881825710

[14] Manthiram, A., Kim, J. H., Kim, Y.N., Lee, K.T. (2011). Crystal chemistry and properties of mixed ionic-electronic conductors. Journal of Electroceramics, 27(2): 93-107. https://doi.org/10.1007/s10832-011-9635-x

[15] Subardi, A., Liao, K.Y., Fu, Y.P. (2019). Oxygen transport, thermal and electrochemical properties of $NdBa_{0.5}Sr_{0.5}Co_2O_{5+\delta}$ cathode for SOFCs. Journal of the European Ceramic Society, 39(1): 30-40. https://doi.org/10.1016/j.jeurceramsoc.2018.01.022

[16] Faro, M.L., Reis, R.M., Saglietti, G.G.A., Oliveira, V.L., Zignani, S.C., Trocino, S., Aricò, A.S. (2018). Solid oxide fuel cells fed with dry ethanol: The effect of a perovskite protective anodic layer containing dispersed Ni-alloy @ FeOx core-shell nanoparticles. Applied Catalysis B: Environmental, 220: 98-110. https://doi.org/10.1016/j.apcatb.2017.08.010

[17] Ritzmann, A.M., Pavone, M., Muñoz-García, A.B., Keithc, J.A., Carter, E.A. (2014). Ab initio DFT+U analysis of oxygen transport in $LaCoO_3$: The effect of Co^{3+} magnetic states. Journal of Material Chemistry A, 2: 8060-8074. https://doi.org/10.1039/C4TA00801D

[18] Pelosato, R., Cordaro, G., Stucchi, D., Cristiani, C., Dotelli, G. (2015). Cobalt based layered perovskites as cathode material for intermediate temperature solid oxide fuel cells: A brief review. Power Sources, 298: 46-67. https://doi.org/10.1016/j.jpowsour.2015.08.034

[19] Chiba, R., Yoshimura, F., Sakurai, Y. (1999). An investigation of $LaNi_{1-x}Fe_xO_3$ as a cathode material for solid oxide fuel cells. Solid State Ionics, 124: 281-288. https://doi.org/10.1016/S0167-2738(99)00222-2

[20] Dicks, A.L., Rand, D.A. (2018). Fuel Cell Systems Explained. John Wiley & Sons.

[21] Singhal, S.C., Kendall, K. (2003). High-Temperature Solid Oxide Fuel Cells: Fundamentals, Design, and Applications. Elsevier.

[22] Mahato, N., Banerjee, A., Gupta, A., Omar, S., Balani, K. (2015). Progress in material selection for solid oxide fuel cell technology: A review. Progress in Materials Science, 72: 141-337. https://doi.org/10.1016/j.pmatsci.2015.01.001

[23] Singhal, S.C. (2000). Advances in solid oxide fuel cell technology. Solid-State Ionics, 135(1-4): 305-313. https://doi.org/10.1016/S0167-2738(00)00452-5

[24] López-Robledo, M.J., Laguna-Bercero, M.A., Larrea, A., Orera, V.M. (2018). Reversible operation of microtubular solid oxide cells using $La_{0.6}Sr_{0.4}Co_{0.2}Fe_{0.8}O_{3-\delta}$-$Ce_{0.9}Gd_{0.1}O_{2-\delta}$ oxygen electrodes. Journal of Power Sources, 378: 184-189. https://doi.org/10.1016/j.jpowsour.2017.12.035

[25] Bessel, C.A., Laubernds, K., Rodriguez, N.M., Baker, R.T.K. (2001). Graphite nanofibers as an electrode for fuel cell applications. The Journal of Physical Chemistry B, 105(6): 1115-1118. https://doi.org/10.1021/jp003280d

[26] Meadowcroft, D.B. (1970). Low-cost oxygen electrode material. Nature, 226(5248): 847-848. https://doi.org/10.1038/226847a0

[27] Wang, H.Q., Lai, F.Y., Li, Y., Zhang, X.H., Huang, Y.G., Hu, S.J., Li, Q.Y. (2015). Excellent stability of spinel $LiMn_2O_4$-based cathode materials for lithium-ion batteries. Electrochimica Acta, 177(2): 290-297. https://doi.org/10.1016/j.electacta.2015.02.027

[28] Siqueira Jr, J.M., Machado, C.T., Quattrociocchi, D.S.G., Garrido., F.M.S., da Costa. L.M., Ponzioa, E.A., Ferreira, G.B., Resende, J.A.L.C. (2020). Experimental and theoretical study of $LiMn_2O_4$ synthesized by the solution combustion method using corn starch as fuel. Journal of the Brazilian Chemical Society, 31(2): 381-393. http://dx.doi.org/10.21577/0103-5053.20190192